APPLIED SCIENCES AND ENGINEERING

Dissociating stable nitrogen molecules under mild conditions by cyclic strain engineering

Gao-Feng Han[1]*, Xiang-Mei Shi[2]*, Seok-Jin Kim[1], Jeonghun Kim[3], Jong-Pil Jeon[1], Hyuk-Jun Noh[1], Yoon-Kwang Im[1], Feng Li[1], Young Rang Uhm[4], Chul Sung Kim[3], Qing Jiang[2]†, Jong-Beom Baek[1]†

All quiet on the nitrogen front. The dissociation of stable diatomic nitrogen molecules (N_2) is one of the most challenging tasks in the scientific community and currently requires both high pressure and high temperature. Here, we demonstrate that N_2 can be dissociated under mild conditions by cyclic strain engineering. The method can be performed at a critical reaction pressure of less than 1 bar, and the temperature of the reaction container is only 40°C. When graphite was used as a dissociated N* receptor, the normalized loading of N to C reached as high as 16.3 at/at %. Such efficient nitrogen dissociation is induced by the cyclic loading and unloading mechanical strain, which has the effect of altering the binding energy of N, facilitating adsorption in the strain-free stage and desorption in the compressive strain stage. Our finding may lead to opportunities for the direct synthesis of N-containing compounds from N_2.

INTRODUCTION

If a process for dissociating stable diatomic nitrogen molecules (N_2) into relatively inert organic substances was available, it could replace the use of traditional reactive nitrogen compounds as a nitrogen source and lead to a notable reduction in reactive nitrogen pollution (*1*, *2*). However, present state-of-the-art techniques and even enzyme nitrogenase are still unable to practically realize this concept. The underlying reasons are the strong dissociation energy (941 kJ mol^{-1}), high first ionization energy (1503 kJ mol^{-1}), and short N≡N triple bond (1.098 Å) of the N_2 molecule, which make it stably inert, and pose important challenges to synthesis (*2*–*6*). According to the Brønsted-Evans-Polanyi relation, the high activation energy of N_2 dissociation means that nitrogen atoms require a stronger binding energy ($|\Delta E|$) on the surface of a transition metal (*7*, *8*). However, the strong binding energy inevitably results in a higher desorption energy in terms of scaling relations (*7*–*9*). As a result, N_2 dissociation usually requires very harsh conditions. For example, when Fe is used as a catalyst, the Fe–N bonding is so strong that a reconstructed "surface nitride" is formed (*10*–*12*). Accordingly, a temperature of a few hundreds of degrees Celsius is usually required for the desorption of N atoms adsorbed on the surface of Fe (*2*, *10*, *13*–*15*).

Breaking the scaling relations has become an attractive approach for overcoming such harsh conditions. Frequently used methods use an external stimulus, such as an electric arc (*2*) or plasma (*16*, *17*), which can change the vibrational energy of N_2. However, those methods do not change the catalyst itself, and the doping level of N is as low as 1% (*2*, *16*, *17*). Another well-studied way to break the scaling law involves strain engineering (*18*–*24*). According to *d*-band theory, strain can change the *d*-band center, which subsequently influences the activity of the catalyst (*25*). Recently, Peterson and colleagues showed how strain breaks this constraint using a mechanics-based eigenstress model to theoretically characterize the effect of strain on adsorbate-catalyst bonding (*18*).

Here, we demonstrate that N_2 can be easily dissociated under mild conditions via cyclic strain engineering. N_2 is first dissociatively adsorbed onto the activated surface of Fe balls [hardened steel with 99 weight % (wt %) Fe], to form adsorbed nitrogen atoms (N*), which are then desorbed by compressive strain due to drastic collisions by ball milling. The dissociated N* can then directly react with other active species, forming relatively inert organic substances, without having to resort to reactive nitrogen compounds as the N source. In this study, we used graphite as receptor to accommodate the N* atoms. The nitrogenation, unzipping, and delamination of the graphite simultaneously proceed, forming N-doped graphitic nanoplatelets (GNPs). The concept of cyclic strain engineering can also be extended to other reactions and used to mitigate harsh reaction conditions.

RESULTS AND DISCUSSION

We determined that direct nitrogenation of GNP can be accomplished under mild conditions via N_2 dissociation, using mechanochemical methods. The successful nitrogenation of the GNP was verified by a series of characterizations (fig. S1 and table S1). The kinetics of nitrogenation at the free edge sites of GNP were first studied in this work.

Examining the N content as a function of reaction time, we found that the rate of increase in N exponentially decayed and saturated with longer reaction times (Fig. 1A and figs. S2 and S3). When the ball milling time is 3 hours, the calculated fixation yield is 272.3 and 459.7 μg cm^{-2} $hour^{-1}$ for Φ 3 mm and Φ 5 mm Fe balls, respectively. Here, N content was determined using the most reliable method, elemental analysis. We did not directly use the consumed volume of N_2 ($V_{consumed}$) to determine content, because, in addition to chemically fixed N_2 (V_{chem}), a small amount of N_2 was physically adsorbed (V_{phys}) owing to the increase in surface area during unzipping and delamination of graphite. Namely, $V_{consumed}$ is equal to V_{phys} plus V_{chem}. However, the $V_{consumed}$ was a sufficient metric for comparing samples, which were prepared under the same ball-milling conditions.

We also noticed that there was an initial activation process: the N content was not zero at reaction time 0 hours after extrapolation. When larger Fe balls were used to provide higher kinetic energy, this period of initial activation was shortened. The existence of an activation process implies that the mechanism of N_2 dissociation is not a direct cleavage reaction, because direct cleavage does not require an incubation period.

[1]School of Energy and Chemical Engineering/Center for Dimension-Controllable Organic Frameworks, Ulsan National Institute of Science and Technology (UNIST), Ulsan 44919, South Korea. [2]Key Laboratory of Automobile Materials (Jilin University), Ministry of Education, and School of Materials Science and Engineering, Jilin University, Changchun 130022, China. [3]Department of Physics, Kookmin University, Seoul 02707, South Korea. [4]Radioisotope Research Division, Korea Atomic Energy Research Institute (KAERI), Daejeon 34057, South Korea.
*These authors contributed equally to this work.
†Corresponding author. Email: jbbaek@unist.ac.kr (J.-B.B.); jiangq@jlu.edu.cn (Q.J.)

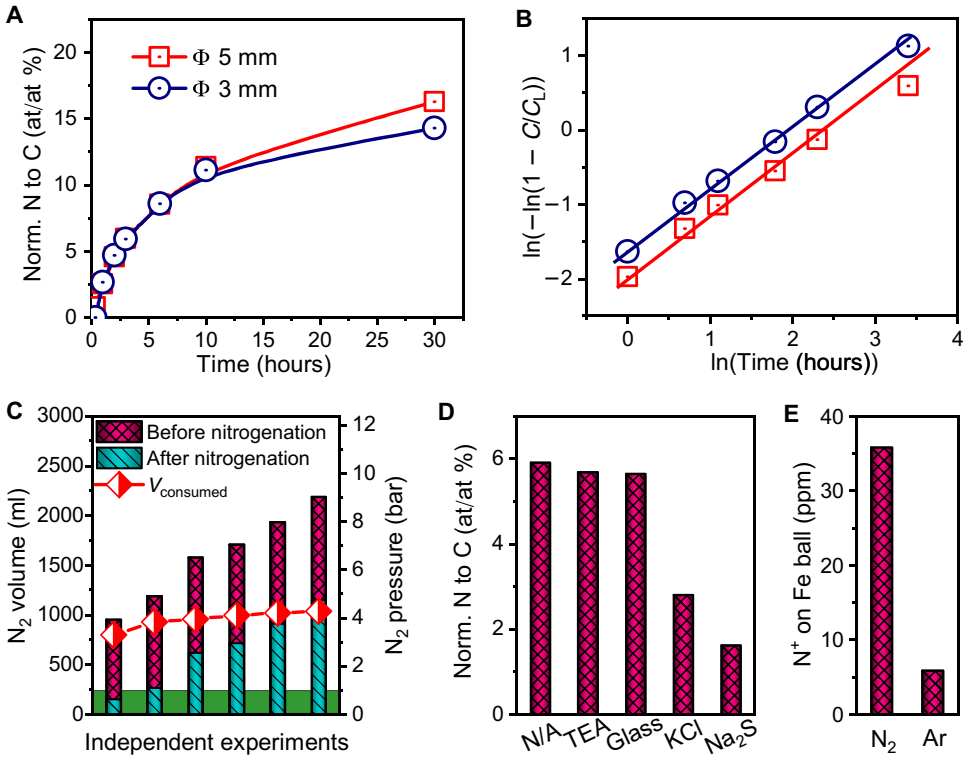

Fig. 1. The reactivity of N_2 dissociation. (**A**) Nitrogen content in the as-prepared nitrogenated GNP as a function of time. (**B**) The corresponding Avrami equation of reaction kinetics. *C* is the concentration of N, and C_L the limiting concentration of N. (**C**) The nitrogen consumption ($V_{consumed}$) as a function of different charging pressures. (**D**) The poisoning experiments. Triethanolamine (TEA), glass powder, KCl, and Na_2S were separately added as interference. (**E**) The self-nitrogenating phenomenon of the Fe ball is characterized by the N^+ content on the surface of the Fe balls. The N^+ content was determined by time-of-flight secondary ion mass spectrometry. ppm, parts per million.

This was further proved by analyzing the data with the Avrami equation, which is a typical kinetic equation that needs an activation process (*26*). The well-matched linear relation verified that the N fixation in the present experiments followed the Avrami equation (Fig. 1B). The fixed N content is linearly dependent on the rotation speed (fig. S4A).

Next, we studied the role of graphite loading on the N_2 dissociation. The normalized $V_{consumed}$ showed that N_2 dissociation increased as graphite loading decreased (fig. S4B). Worn-off Fe nanoparticle debris in the GNP increased as well (fig. S4B). The results indicate that the enhanced N_2 consumption was due to an increase in normalized Fe sites, which generate more N*.

Then, the effect of N_2 pressure on the reaction was studied. The results showed that N_2 pressure had little influence on the reaction (Fig. 1C). The finding further indicates that the N atoms fixed in the GNP are not involved in direct N_2 cleavage at the free edge sites of the cracked GNP. The critical reaction pressure was determined by the lowest remnant pressure in the container. While the charged pressure was 3.0 bar, the remnant gas in the container was less than 1 bar. This means that the critical reaction pressure may be less than 1 bar. To rule out interference from the physically adsorbed N_2 (V_{phys}), we designed an elaborate experiment. The graphite was first pretreated by ball milling for 6 hours in N_2 (8.0 bar) to provide the same surface area. Then, we checked the critical reaction pressure twice again, which was further verified to be less than 1 bar (fig. S4, C and D). The lower critical pressure means the higher fixation efficiency in our method. For example, when the initial pressure is 8 bar, the maximum fixation efficiency can reach up to 90%.

We also studied the influence of the temperature in the reaction container. The temperature in the container was controlled by programming the milling time. Our experiments demonstrated that short milling time and long cooling time (where maximum temperature in the container reached 40°C) resulted in nearly the same N content as long milling time and short cooling time (75°C, fig. S4E). The results indicate that the reaction can proceed at near-ambient temperature without any direct relation to the container temperature. The possible reason is that the local temperature during collisions dominantly affects the N_2 dissociation (vide infra).

As a comparison experiment, ZrO_2 balls were used instead of Fe balls. The amount of fixed nitrogen in GNP reached approximately 50% at equivalent conditions (fig. S5A). Since the oxinitride was formed during the ball-milling process (fig. S5B), the ZrO_2 balls can also have catalytic activity to some extent. In addition, the collision-induced local temperature should be distinctively different between Fe and ZrO_2 balls because the Fe balls are elastic and their elastic deformation could absorb the kinetic energy to a great extent. On the contrary, the ZrO_2 balls are inelastic. Thus, the local temperature generated by ZrO_2 balls should be much higher than that by Fe balls, because of the smaller contact area and the less contact time. Furthermore, the cleavage efficiency of graphite by ZrO_2 balls is the higher owing to the smaller surface energy. If the dissociation of N_2 follows the direct dissociation mechanism, the N content of the GNP prepared by ZrO_2 balls should be higher than that by Fe balls. It is simply because ZrO_2 balls generate the higher local temperature and the more active sites on GNP to accommodate N*. However, the result does not follow this hypothesis, suggesting that the experiment

with the ZrO_2 balls is not an effective comparison. A convincing mechanism study should be done by means of other methods.

A series of poisoning experiments were also conducted to study the reaction mechanism. Small amounts of triethanolamine (TEA), glass powders, potassium chloride (KCl), and sodium sulfide (Na_2S) were individually added to sample mixtures before ball milling (Fig. 1D and fig. S6). The TEA and glass powders had nearly no influence on N_2 dissociation. However, KCl and Na_2S severely poisoned the N_2 dissociation. Cl and S are notoriously known to poison active Fe sites (*2*, *11*). The poisoning experiments clarified that the activated Fe sites on the balls play a pivotal role in the N_2 dissociation.

A self-nitrogenating protection phenomenon also occurred during ball milling (fig. S7). The surface strength of the Fe balls against friction was improved under certain conditions, as estimated by the amount of worn-off Fe debris in the GNP. For example, the Fe content of GNP in argon (Ar) was 2.6 times higher than that in N_2 under the same ball-milling conditions (10 hours, Φ 5-mm Fe balls) (fig. S7). It is known that dissolved N atoms on the surface of Fe can mitigate abrasion, due to solid solution hardening, and also strengthen the antioxidation property (*27*). The N concentration on the surface of the Fe balls had a direct influence on the self-nitrogenating phenomenon. However, when we characterized the N concentration on the surface of the Fe balls, we encountered a problem, in that the N data overlapped that of remnant carbon species. To separate the two different kinds of N, we used a sensitive time-of-flight secondary ion mass spectrometry (TOF-SIMS) technique. The TOF-SIMS results showed that the N^+ on the Fe balls after ball milling in N_2 was 6.1 times higher than that on the original Fe balls (Fig. 1E). The increased nitrogen content on the surface of the Fe balls helps explain the N_2 dissociation mechanism.

To study the underlying mechanism and rule out the interference of carbon species, a transfer experiment was designed. Briefly, we first used Fe powders to dissociatively adsorb nitrogen [Fe(N*)]. Then, the adsorbed N* was transferred to the GNP by ball milling the N ultrasaturated Fe(N*) together with graphite (denoted as Fe + GNP). As shown in Fig. 2A, the x-ray powder diffraction (XRD) patterns show that the Fe (N*) shifts to low angle relative to the Fe + GNP mixture and pure Fe (JSPDF: 06-0696). The result indicates that the lattice constant is enlarged by the interstitial N atoms in octahedral holes (*28*). The Fe (110) facet of Fe + GNP has the same angle as pure Fe, which confirms that the Fe(N*) has successfully desorbed the N*.

The XPS determined that the surface concentration of N was 18.8 atomic % (at %) relative to Fe, and the bulk concentration of N was calculated to be 3.5 at % (*28*), based on the shift in the XRD patterns (see Supplementary Text). The result demonstrates that the N* atoms are ultrasaturated in the Fe powders in comparison with the thermal-equilibrium bulk concentration of 2.05×10^{-6} (*15*).

The radial distribution functions (Fig. 2B), which were derived from the extended x-ray absorption fine structure (EXAFS) measurements, agreed well with the XRD results obtained by directly monitoring the Fe–Fe and Fe–N bonds (*29*). Some Fe–C bonds were found in the Fe + GNP mixtures, which correspond to the minor peaks in XRD patterns.

The Mossbauer spectroscopy results (Fig. 2C) demonstrated that N atoms were present as nitrides (Fe_4N) in Fe(N*) (*29*–*32*). The Fe_4N

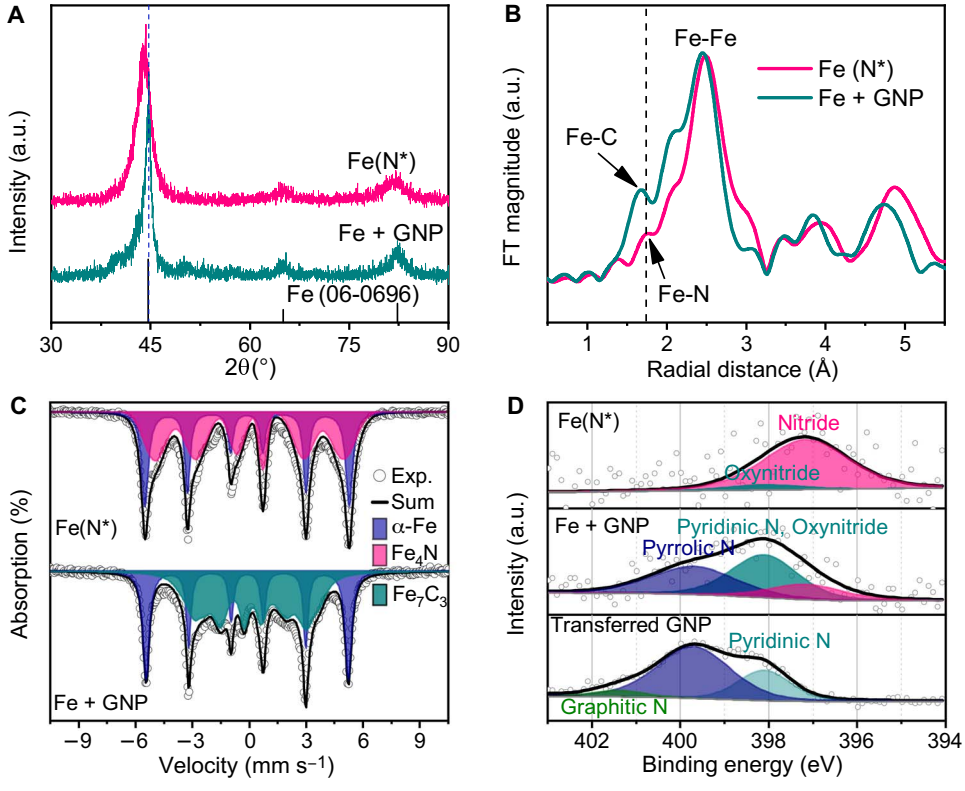

Fig. 2. The transfer experiments. (**A**) XRD patterns of the nitrogenated Fe [Fe(N*)] and its mixture with GNP (Fe + GNP). (**B**) The radial distribution function, determined by EXAFS. (**C**) Mossbauer spectroscopy results. (**D**) The transfer process of N from nitride Fe–N to organic C–N, recorded by high-resolution observation of N 1s. a.u., arbitrary units.

disappeared in the Fe + GNP, and the carbide Fe_7C_3 was formed (*30*, *33*). The transfer process of N* was also explicitly recorded by the chemical environment of N 1s (Fig. 2D). N was successfully transferred from the nitride Fe–N bond to the organic C–N bond (fig. S8). Some oxynitrides were formed because of oxidation after exposure to air.

Intuitively, the dissociation of N≡N triple bond is very difficult, because of its high dissociation energy. However, the reaction over a catalyst can avoid this problem, since the energy gain associated with the formation of Fe–N bonds overcompensates the dissociation energy. The dissociative adsorption of N_2 has actually become exothermic (*2*). The maximum energy barrier to form Fe(N*) is only about 0.1 eV (*12*). At low temperature, since the vibrational entropy is very small, the desorption of N* dominates the reaction more than the formation of Fe(N*) due to the strong Fe–N bonds (1.5 eV).

Now, considering the low container temperature (40°C), the question arises as to how the reaction proceeds. According to the hotspot theory (*26*), collision processes of 10^{-4} to 10^{-3} s can produce local surface temperatures of higher than 700°C per square micrometer. However, since graphite is a good solid lubricant and Fe balls are elastic, the local temperature can be largely discounted. At low temperature, the local temperature can only partially drive the N* out of the Fe(N*). Nevertheless, the increased local temperature is beneficial, by accelerating the N* dissociation kinetics.

A clue to unravel the underlying mechanism can be found in the phenomenon of forging, which is a technique of repeatedly peening a steel piece to reduce impurities. We considered the impact of compressive strain on the binding energy. Because such collisions happen in a very short time frame, the lattice does not have enough time to fully relax. To describe this partially relaxed phenomenon, we calculated the two extreme cases, relaxed and unrelaxed.

Density functional theory (DFT) calculations were used to determine the functions between the applied strain and the energy of the N atom on the Fe substrates, as illustrated in Fig. 3. The formation/adsorption energy increased as the strain increased for both the bulk and surface models. The formation energy was nearly zero, when the applied strain was free in the bulk model (Fig. 3A). This means that the structure is stable, because the N atoms can raise the entropy of pure Fe. However, when the applied strain was increased, N atoms were easily segregated from the bulk, owing to the high positive formation energy.

The surface model case was distinctive, because its adsorption energy was negative (Fig. 3B). This means that N* can be stably adsorbed on the Fe(110) surface. When the applied strain was zero for the surface model, adsorption was very strong (about −1.5 eV), and thus the N* was irreversibly adsorbed onto the Fe surface, and even Fe nitrides were formed. When a strain of 10% was applied, the adsorption energy exponentially receded to −0.1 eV in the unrelaxed surface model. The N* can easily desorb from the Fe surface because of this weakened adsorption energy.

Now, the whole underlying mechanism can be interpreted using a cyclic strain engineering model (Fig. 4). First, mechanical energy is

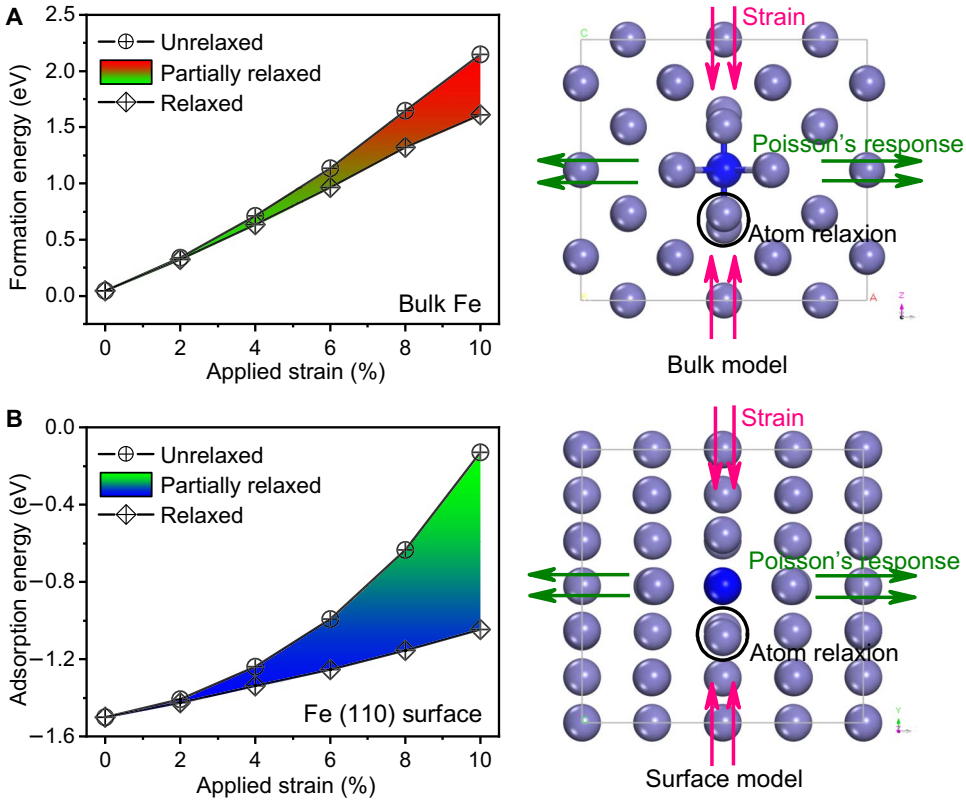

Fig. 3. Theoretical analysis of the formation and adsorption energy as a function of applied strain. (**A**) The Fe bulk model. (**B**) The Fe (110) surface model. The relaxed model is fully relaxed. The unrelaxed model adopts the same Poisson's responses as those in the relaxed model except that the atom positions were not relaxed. A lower energy value (ΔE) corresponds to stronger adsorption of N atoms on the Fe substrate. A higher ΔE value indicates easier segregation of nitrogen atoms from the corresponding Fe system.

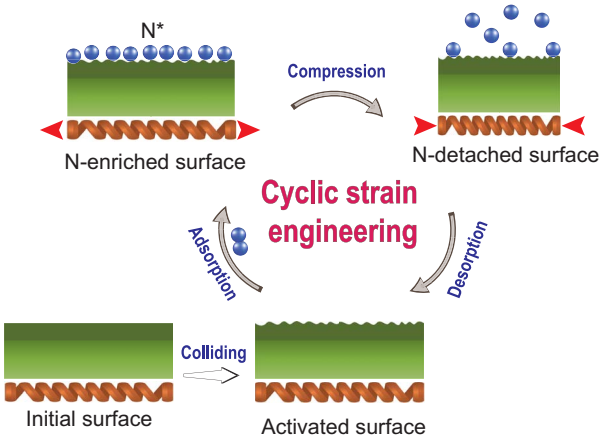

Fig. 4. N_2 dissociation via cyclic strain engineering. The repeated collisions of the Fe balls result in the activation of the surface. The originally flat and passivated surfaces are converted into nanocrystalline structures with highly active sites. N_2 dissociation occurs on the Fe atoms of the activated surface. The shock of compression reduces the N* adsorption energy, and the N* atoms are detached from the surface. The vacant sites on the activated surface will adsorb new N* atoms at the strain-free stage, and the cyclic strain process will repeat until the collisions stop.

transformed into elastic energy in the lattice defects, and into structural disordering, or it can be released by plastic transformation by the rearrangement of the crystallographic lattice (*27*, *34*). The repeated collisions transform the passivated surface of the Fe balls into activated surfaces. This explains why the reaction needs an initial activation period and why bigger Fe balls, with higher kinetic energy per ball, reduce the activation time. The activated surface with a high number of defects facilitates the dissociation of N_2 (*35*) and speeds up the diffusion of N atoms (*27*). Then, as the compressive strain reduces the adsorption energy, the adsorbed nitrogen atoms are desorbed. Last, the vacated Fe sites, which, in the strain-free stage, have higher adsorption energy, quickly adsorb new N* once again via N_2 dissociation. N_2 is dissociatively adsorbed in the strain-free stage, and the N* is desorbed in the compressive strain stage. Cyclic strain is formed and successively provides dissociated N* atoms.

The desorbed N* atoms react with the free edge sites of the GNP to form N-doped carbon materials. While the mechanism for N* fixation at the edges of GNP is not the focus of this work, here, we briefly introduce the N* fixation process at the edge sites. The desorbed N*, or following combination with unbonded C* to form C≡N and C_3N radicals, reacts with the reactive dangling edge sites (*36*). This method can be easily extended to other carbon materials, such as carbon black (CB; fig. S9). These kinds of N-doped carbon materials have received considerable attention in the research community, due to their wide applications in catalysis, including oxygen reduction reactions and dehydrogenation reactions, and in substrates for other catalysts.

MATERIALS AND METHODS

The influence of milling time

The nitrogenation of GNP was realized by a mechanochemical ball-milling method. The typical experiment was conducted on a planetary ball-milling machine (Pulverisette 6, Fritsch GmbH) at a rotation speed of 500 rpm. In brief, graphite (15 g, 100 mesh, 99.9995%, Alfa Aesar, product number: 14735) and Fe balls (hardened steel with 99 wt % Fe, 500 g, Φ = 3 mm or Φ = 5 mm) were loaded in a ball-mill container (250 ml). Before ball milling, air in the container was first evacuated by a vacuum pump, and then the container was purged with N_2 at least four times to remove residual air. Last, the container was charged with N_2 gas (UHP, 99.999%, N50, KOSEM, Korea). The total milling times were $^1/_3$, 1, 2, 3, 6, 10, 20, and 30 hours. For the cases with milling times of 20 and 30 hours, N_2 charging was conducted two and three times, respectively, after every 10 hours of milling to supply enough N_2. During ball milling, rotation is stopped for 10 min per 1 hour of milling to release the heat induced by mechanical friction. Safety note: Samples with longer ball-milling times, greater than 10 hours with Φ 5-mm Fe balls, require special attention when collecting GNP, because of violent sparking caused by oxidation after exposure to air. We recommend using aluminum foil to collect the GNP.

The poisoning experiments

The purpose of the poisoning experiments was to investigate the reaction mechanism. TEA (150 μl, GC ≥ 99.0%, Sigma-Aldrich, product number: 33729), glass powders (0.3 g, Thomas Scientific), potassium chloride (KCl, 0.3 g; ACS, 99.0 to 100.0%; Alfa Aesar, product number: 11595), and anhydrous sodium sulfide (Na_2S, 0.3 g, Sigma-Aldrich, product number: 407410) were separately added into the container together with graphite (15 g). The graphite was then ball-milled with Fe balls (Φ = 5 mm) in N_2 (8 bar) at a rotation speed of 500 rpm for 3 hours. Last, the remnant gas was collected by water displacement method to calculate the consumed N_2 gas. Safety note: After the addition of KCl or Na_2S, caution should be exercised when collecting samples due to violent sparking by oxidation after exposure to air. We recommend using aluminum foil to collect GNP.

The influence of rotation speed

The selected rotation speeds were 500, 400, 300, and 200 rpm, respectively. The graphite was ball-milled with Fe balls (Φ = 3 mm) in N_2 (8 bar) for 6 hours.

The influence of graphite loading

The selected loading amounts of graphite were 5, 10, 15, and 20 g. The graphite was ball-milled with Fe balls (Φ = 5 mm) in N_2 (8 bar) at a rotation speed of 500 rpm for 3 hours.

The effect of reaction pressure and critical reaction pressure

The N_2 charging pressures were 8.1, 7.0, 6.2, 5.5, 4.0, and 3.0 bar. The charged N_2 pressure was measured by a pressure gauge (MODEL 801, the Harris Calorific Co., USA). It should be noted that the true pressure in the container is equal to the charged pressure plus 1 bar. The nitrogenation method was ball milling graphite with Fe balls (Φ = 5 mm) in N_2 (8 bar) at a rotation speed of 500 rpm for 3 hours.

The critical reaction pressure was thought to be the smallest remnant pressure in the container. The amount of physically adsorbed N_2 (V_{phys}) was first ruled out. The graphite was first pretreated by milling for 6 hours in N_2 (8.0 bar) to produce an equivalent surface area for each GNP. Then, the container was filled with N_2 gas (approximately 2.0 bar), and milling was conducted for 3 hours. We checked two times separately, and the results agreed well with each other. It should be pointed out that the volume of N_2 gas measured by water displacement does not reflect the void in the container.

The influence of container temperature

The temperature of the container was controlled by cooling time. The cooling time was 30 min for every 10 min of ball milling. The

nitrogenation method was ball milling of graphite with Fe balls (Φ = 5 mm) in N_2 (8 bar) at a rotation speed of 500 rpm for 3 hours.

Ball milling with ZrO_2 balls

The graphite was ball-milled with ZrO_2 balls (Φ = 3 mm) at a rotation speed of 353 rpm in N_2 (8 bar) for 180,000 cycles.

The extension to other carbon materials

CB was also tested as a N acceptor. The nitrogenation CB was carried out by ball milling CB (10 g, acetylene, 100% compressed, 99.9+%, Alfa Aesar, product number: 45527) with Fe balls (Φ = 5 mm) in N_2 (8 bar) at a rotation speed of 500 rpm for 30 hours. The N_2 gas was recharged every 10 hours.

The transfer experiments

Fe nitrogenation [Fe(N*)] was conducted by ball milling Fe powder (69.83 g, fine powder, ≥99%, Sigma-Aldrich, product number: 44890) with Fe balls (Φ = 5 mm) in N_2 (8 bar) at a rotation speed of 500 rpm for 100 hours. The N_2 gas was recharged after every 20 hours of milling. The cooling time was 30 min after ball milling for every 10 min to avoid raising the temperature in the container too high.

Then, the as-prepared Fe(N*) was taken out in an argon-filled glove box to avoid any oxidation. Fe(N*) (60 g) was milled together with 5 g of graphite for 10 hours at a rotation speed of 500 rpm in Ar gas (1 bar, UHP, 99.999%, N50, KOSEM Corp., Korea). This as-prepared mixture was designated Fe + GNP.

Last, the Fe in the mixture was leached out using 20% aqueous HCl (ACS reagent, 37%, Sigma-Aldrich, product number: 320331) for 24 hours. After rinsing with distilled water, the GNP was freeze-dried at −120°C for easy transfer.

Computational methods

DFT calculations were performed with the CASTEP module (*37*) in the Materials Studio package using on-the-fly–generated ultrasoft pseudopotentials. The GGA-PW91 function (*12*, *38*) with a cutoff energy of 400 eV was used and the Monkhorst-Pack *k*-point separation was about 0.04 $Å^{-1}$. Geometries were relaxed until the maximum forces were below 0.03 eV $Å^{-1}$.

The optimized lattice parameter of the Fe unit cell was 2.831 Å, agreeing well with the experimental value of 2.867 Å. The effect of strain on the segregation of nitrogen atoms for bulk Fe–N alloy was calculated with a 3 by 3 by 3 supercell of bulk Fe, where only the elastic regime was considered. A series of uniaxial compressive strains were applied to the bulk Fe by modifying the lattice parameter in the *z* direction, while the supercell in other directions was fully relaxed. The fully relaxed model was labeled the relaxed bulk model. The unrelaxed bulk model adopted the same Poisson's responses as the relaxed bulk model except that the atom positions were not relaxed. Namely, the unrelaxed model was obtained by linearly compressing/stretching the strain-free model to the lattice of the relaxed bulk model.

For the surface model, we selected the Fe (110) facet as the study surface, although the (110) facets were reported to be the most inactive surface (*10*, *39*). This is because (110) has the largest quantity of facets and the lowest surface energy facets in the body center cubic structure of Fe. Here, we built a 2 by 3 rectangular slab of the (110) surface with a thickness of three atomic layers. The bottom layer was fixed, and a vacuum layer of 15 Å was added in the *z* direction to avoid interactions between periodic slabs. We also applied uniaxial compressive strain in the *y* direction. The slab parameters and atomic positions were adjusted according to the calculated bulk Poisson's responses (*18*).

The formation (solution) energies of nitrogen atoms in the bulk Fe and the adsorption (binding) energies on the Fe (110) surface were described in the same manner

$$\Delta E = E_{\text{total}} - E_{\text{Fe}} - 1/2E_{\text{N2}} \quad (1)$$

where E_{total}, E_{Fe}, and E_{N2} are the total energies of the Fe systems (bulk or surface model) with a nitrogen atom, Fe systems, and molecular N_2, respectively. The higher value of ΔE indicates easier segregation of the nitrogen atoms from the Fe system.

Since the Fe is compressed along the *z* axial direction, Poisson's ratio was calculated as follows:

$$\nu = -d\varepsilon_{\text{trans}}/d\varepsilon_{\text{axial}} = -d\varepsilon_x/d\varepsilon_z = -d\varepsilon_y/d\varepsilon_z \quad (2)$$

where ν is the resulting Poisson's ratio, $\varepsilon_{\text{trans}}$ is the transverse strain (positive for the axial compression), and $\varepsilon_{\text{axial}}$ is the axial strain (negative for the axial compression).

SUPPLEMENTARY MATERIALS

Supplementary material for this article is available at http://advances.sciencemag.org/cgi/content/full/5/11/eaax8275/DC1

Supplementary Materials and Methods

Supplementary Text

Fig. S1. Comparison of the as-prepared samples in N_2 and Ar.

Fig. S2. GNPs after different nitrogenation times.

Fig. S3. GNPs after different nitrogenation times.

Fig. S4. Studies of the rotation speed of ball milling, the loading amount of graphite, the critical reaction pressure, and temperature of the ball-mill container.

Fig. S5. Ball milling by ZrO_2 balls.

Fig. S6. The poisoning experiments.

Fig. S7. The self-nitrogenating protection phenomenon of Fe balls.

Fig. S8. The transfer experiments.

Fig. S9. Extension to other carbon materials.

Table S1. Elemental analysis of the GNP.

REFERENCES AND NOTES

1. E. Boyle, Nitrogen pollution knows no bounds. *Science* **356**, 700–701 (2017).
2. M. Appl, *Ammonia: Principles and Industrial Practice* (Wiley-VCH Verlag GmbH, 1999).
3. D. J. Knobloch, E. Lobkovsky, P. J. Chirik, Dinitrogen cleavage and functionalization by carbon monoxide promoted by a hafnium complex. *Nat. Chem.* **2**, 30–35 (2010).
4. G.-F. Chen, X. Cao, S. Wu, X. Zeng, L.-X. Ding, M. Zhu, H. Wang, Ammonia electrosynthesis with high selectivity under ambient conditions via a Li^+ incorporation strategy. *J. Am. Chem. Soc.* **139**, 9771–9774 (2017).
5. L. Zhang, L.-X. Ding, G.-F. Chen, X. Yang, H. Wang, Ammonia synthesis under ambient conditions: Selective electroreduction of dinitrogen to ammonia on black phosphorus nanosheets. *Angew. Chem. Int. Ed. Engl.* **58**, 2612–2616 (2019).
6. H. Cheng, L.-X. Ding, G.-F. Chen, L. Zhang, J. Xue, H. Wang, Molybdenum carbide nanodots enable efficient electrocatalytic nitrogen fixation under ambient conditions. *Adv. Mater.* **30**, e1803694 (2018).
7. A. Logadottir, T. H. Rod, J. K. Nørskov, B. Hammer, S. Dahl, C. J. H. Jacobsen, The Brønsted–Evans–Polanyi relation and the volcano plot for ammonia synthesis over transition metal catalysts. *J. Catal.* **197**, 229–231 (2001).
8. F. Calle-Vallejo, J. I. Martínez, J. M. García-Lastra, J. Rossmeisl, M. T. M. Koper, Physical and chemical nature of the scaling relations between adsorption energies of atoms on metal surfaces. *Phys. Rev. Lett.* **108**, 116103 (2012).
9. F. Abild-Pedersen, J. Greeley, F. Studt, J. Rossmeisl, T. R. Munter, P. G. Moses, E. Skúlason, T. Bligaard, J. K. Nørskov, Scaling properties of adsorption energies for hydrogen-containing molecules on transition-metal surfaces. *Phys. Rev. Lett.* **99**, 016105 (2007).
10. F. Bozso, G. Ertl, M. Weiss, Interaction of nitrogen with iron surfaces: II. Fe(110). *J. Catal.* **50**, 519–529 (1977).

11. C. N. R. Rao, G. R. Rao, Nature of nitrogen adsorbed on transition metal surfaces as revealed by electron spectroscopy and cognate techniques. *Surf. Sci. Rep.* **13**, 221–263 (1991).
12. J. J. Mortensen, M. V. Ganduglia-Pirovano, L. B. Hansen, B. Hammer, P. Stoltze, J. K. Nørskov, Nitrogen adsorption on Fe(111), (100), and (110) surfaces. *Surf. Sci.* **422**, 8–16 (1999).
13. P. Stoltze, J. K. Nørskov, Bridging the "pressure gap" between ultrahigh-vacuum surface physics and high-pressure catalysis. *Phys. Rev. Lett.* **55**, 2502–2505 (1985).
14. J. G. Chen, R. M. Crooks, L. C. Seefeldt, K. L. Bren, R. M. Bullock, M. Y. Darensbourg, P. L. Holland, B. Hoffman, M. J. Janik, A. K. Jones, M. G. Kanatzidis, P. King, K. M. Lancaster, S. V. Lymar, P. Pfromm, W. F. Schneider, R. R. Schrock, Beyond fossil fuel–driven nitrogen transformations. *Science* **360**, eaar6611 (2018).
15. F. Bozso, G. Ertl, M. Grunze, M. Weiss, Interaction of nitrogen with iron surfaces: I. Fe(100) and Fe(111). *J. Catal.* **49**, 18–41 (1977).
16. P. Mehta, P. Barboun, F. A. Herrera, J. Kim, P. Rumbach, D. B. Go, J. C. Hicks, W. F. Schneider, Overcoming ammonia synthesis scaling relations with plasma-enabled catalysis. *Nat. Catal.* **1**, 269–275 (2018).
17. Y. Wang, Y. Shao, D. W. Matson, J. Li, Y. Lin, Nitrogen-doped graphene and its application in electrochemical biosensing. *ACS Nano* **4**, 1790–1798 (2010).
18. A. Khorshidi, J. Violet, J. Hashemi, A. A. Peterson, How strain can break the scaling relations of catalysis. *Nat. Catal.* **1**, 263–268 (2018).
19. M. Mavrikakis, B. Hammer, J. K. Nørskov, Effect of strain on the reactivity of metal surfaces. *Phys. Rev. Lett.* **81**, 2819–2822 (1998).
20. J. R. Kitchin, J. K. Nørskov, M. A. Barteau, J. G. Chen, Role of strain and ligand effects in the modification of the electronic and chemical properties of bimetallic surfaces. *Phys. Rev. Lett.* **93**, 156801 (2004).
21. M. F. Francis, W. A. Curtin, Mechanical work makes important contributions to surface chemistry at steps. *Nat. Commun.* **6**, 6261 (2015).
22. H. Wang, S. Xu, C. Tsai, Y. Li, C. Liu, J. Zhao, Y. Liu, H. Yuan, F. Abild-Pedersen, F. B. Prinz, J. K. Nørskov, Y. Cui, Direct and continuous strain control of catalysts with tunable battery electrode materials. *Science* **354**, 1031–1036 (2016).
23. P. Strasser, S. Koh, T. Anniyev, J. Greeley, K. More, C. Yu, Z. Liu, S. Kaya, D. Nordlund, H. Ogasawara, M. F. Toney, A. Nilsson, Lattice-strain control of the activity in dealloyed core-shell fuel cell catalysts. *Nat. Chem.* **2**, 454–460 (2010).
24. T. Ling, D.-Y. Yan, H. Wang, Y. Jiao, Z. Hu, Y. Zheng, L. Zheng, J. Mao, H. Liu, X.-W. Du, M. Jaroniec, S.-Z. Qiao, Activating cobalt(II) oxide nanorods for efficient electrocatalysis by strain engineering. *Nat. Commun.* **8**, 1509 (2017).
25. A. Logadottir, J. K. Nørskov, The effect of strain for N_2 dissociation on Fe surfaces. *Surf. Sci.* **489**, 135–143 (2001).
26. P. Balaz, *Mechanochemistry in Nanoscience and Minerals Engineering* (Springer-Verlag, 2008).
27. W. P. Tong, N. R. Tao, Z. B. Wang, J. Lu, K. Lu, Nitriding iron at lower temperatures. *Science* **299**, 686–688 (2003).
28. D. H. Jack, K. H. Jack, Invited review: Carbides and nitrides in steel. *Mater. Sci. Eng.* **11**, 1–27 (1973).
29. A. Zitolo, V. Goellner, V. Armel, M. T. Sougrati, T. Mineva, L. Stievano, E. Fonda, F. Jaouen, Identification of catalytic sites for oxygen reduction in iron- and nitrogen-doped graphene materials. *Nat. Mater.* **14**, 937–942 (2015).
30. X.-X. Bi, B. Ganguly, G. P. Huffman, F. E. Huggins, M. Endo, P. C. Eklund, Nanocrystalline α–Fe, Fe_3C, and Fe_7C_3 produced by CO_2 laser pyrolysis. *J. Mater. Res.* **8**, 1666–1674 (1993).
31. T. Ruskov, S. Asenov, I. Spirov, C. Garcia, I. Mönch, A. Graff, R. Kozhuharova, A. Leonhardt, T. Mühl, M. Ritschel, C. M. Schneider, S. Groudeva-Zotova, Mössbauer transmission and back scattered conversion electron study of Fe nanowires encapsulated in multiwalled carbon nanotubes. *J. Appl. Phys.* **96**, 7514–7518 (2004).
32. G. Shirane, W. J. Takei, S. L. Ruby, Mössbauer study of hyperfine fields and isomer shifts in Fe_4N and $(Fe, Ni)_4N$. *Phys. Rev.* **126**, 49–52 (1962).
33. X.-W. Liu, S. Zhao, Y. Meng, Q. Peng, A. K. Dearden, C.-F. Huo, Y. Yang, Y.-W. Li, X.-D. Wen, Mössbauer spectroscopy of iron carbides: From prediction to experimental confirmation. *Sci. Rep.* **6**, 26184 (2016).
34. Y. Chen, T. Halstead, J. S. Williams, Influence of milling temperature and atmosphere on the synthesis of iron nitrides by ball milling. *Mater. Sci. Eng. A* **206**, 24–29 (1996).
35. K. Honkala, A. Hellman, I. N. Remediakis, A. Logadottir, A. Carlsson, S. Dahl, C. H. Christensen, J. K. Nørskov, Ammonia synthesis from first-principles calculations. *Science* **307**, 555–558 (2005).
36. I.-Y. Jeon, H.-J. Choi, M. J. Ju, I. T. Choi, K. Lim, J. Ko, H. K. Kim, J. C. Kim, J.-J. Lee, D. Shin, S.-M. Jung, J.-M. Seo, M.-J. Kim, N. Park, L. Dai, J.-B. Baek, Direct nitrogen fixation at the edges of graphene nanoplatelets as efficient electrocatalysts for energy conversion. *Sci. Rep.* **3**, 2260 (2013).
37. S. J. Clark, M. D. Segall, C. J. Pickard, P. J. Hasnip, M. I. J. Probert, K. Refson, M. C. Payne, First principles methods using CASTEP. *Zeitschrift für Krist. Cryst. Mater.* **220**, 567–570 (2005).
38. J. P. Perdew, J. A. Chevary, S. H. Vosko, K. A. Jackson, M. R. Pederson, D. J. Singh, C. Fiolhais, Atoms, molecules, solids, and surfaces: Applications of the generalized gradient approximation for exchange and correlation. *Phys. Rev. B. Condens. Matter.* **46**, 6671–6687 (1992).
39. N. D. Spencer, R. C. Schoonmaker, G. A. Somorjai, Iron single crystals as ammonia synthesis catalysts: Effect of surface structure on catalyst activity. *J. Catal.* **74**, 129–135 (1982).

Acknowledgments: We are grateful for the use of the Pohang Accelerator Laboratory (6D UNIST-PAL beamline, South Korea). **Funding:** This work was supported by the Creative Research Initiative (CRI, 2014R1A3A2069102), BK21 Plus (10Z20130011057), Science Research Center (SRC, 2016R1A5A1009405), and Mid-Career Researcher (NRF-2017R1A2B2012241) programs through the National Research Foundation (NRF) of Korea, the National Natural Science Foundation of China (no. 51631004), the JLU Science and Technology Innovative Research Team, and the computing resources of High Performance Computing Centers of Jilin University, China. **Author contributions:** J.-B.B. conceived the project and oversaw all the research phases. J.-B.B. and G.-F.H. designed the project. Q.J., X.-M.S., F.L. performed the DFT calculations. S.-J.K., J.-P.J., H.-J.N., Y.-K.I. assisted with the characterization of XAS. C.S.K., Y.R.U., J.K. measured and interpreted Mössbauer spectroscopy. All authors contributed to the writing of the manuscript. Data collection and analysis were conducted by J.-B.B., Q.J., and G.-F.H. **Competing interests:** The authors declare that they have no competing interests. **Data and materials availability:** All data needed to evaluate the conclusions in the paper are present in the paper and/or the Supplementary Materials. Additional data related to this paper may be requested from the authors.

Submitted 26 April 2019
Accepted 16 September 2019
Published 1 November 2019
10.1126/sciadv.aax8275

Citation: G.-F. Han, X.-M. Shi, S.-J. Kim, J. Kim, J.-P. Jeon, H.-J. Noh, Y.-K. Im, F. Li, Y. R. Uhm, C. S. Kim, Q. Jiang, J.-B. Baek, Dissociating stable nitrogen molecules under mild conditions by cyclic strain engineering. *Sci. Adv.* **5**, eaax8275 (2019).

Science Advances

Dissociating stable nitrogen molecules under mild conditions by cyclic strain engineering

Gao-Feng Han, Xiang-Mei Shi, Seok-Jin Kim, Jeonghun Kim, Jong-Pil Jeon, Hyuk-Jun Noh, Yoon-Kwang Im, Feng Li, Young Rang Uhm, Chul Sung Kim, Qing Jiang and Jong-Beom Baek

Sci Adv **5** (11), eaax8275.
DOI: 10.1126/sciadv.aax8275